Journal of Solid State Chemistry 184 (2011) 2472–2477

Contents lists available at ScienceDirect

Journal of Solid State Chemistry

journal homepage: www.elsevier.com/locate/jssc

Syntheses, crystal structures and properties of two unusual pillared-layer 3*d*–4*f* *Ln*–Cu heterometallic coordination polymers

Le-Qing Fan *, Ji-Huai Wu *, Yun-Fang Huang

College of Materials Science and Engineering, the Key Laboratory for Functional Materials of Fujian Higher Education, Huaqiao University, Xiamen, Fujian 361021, PR China

ARTICLE INFO

Article history:
Received 11 May 2011
Received in revised form
11 July 2011
Accepted 17 July 2011
Available online 26 July 2011

Keywords:
Ln–Cu heterometallic coordination polymer
Crystal structure
Luminescent properties
Magnetic properties

ABSTRACT

Two unusual pillared-layer 3*d*–4*f* *Ln*–Cu heterometallic coordination polymers, $\{[Ln_2Cu_5Br_4(IN)_7(H_2O)_6]\cdot H_2O\}_n$ (*Ln*=Eu (**1**) and Gd (**2**), HIN=isonicotinic acid), have been synthesized under hydrothermal conditions, and characterized by elemental analysis, IR, thermal analysis and single-crystal X-ray diffraction. The structure determination reveals that **1** and **2** are isostructural and feature a novel three-dimensional pillared-layer hetrometallic structure built upon the linkages of one-dimensional (1D) linear *Ln*–carboxylate chains, zero-dimensional (0D) *Ln*–carboxylate $Ln_2(IN)_8$ dimers, rare 1D zigzag $[Cu_5Br_4]_n$ inorganic chains and IN^- pillars. In both 3D structures, there are *Ln*–carboxylate layers resulted from the connections of 1D *Ln*–carboxylate chains and 0D $Ln_2(IN)_8$ dimers through O–H···O hydrogen bondings. The luminescent properties of **1** have been investigated. The magnetic properties of **1** and **2** have also been studied.

1. Introduction

There has been growing interest in recent years in the design and synthesis of 3*d*–4*f* heterometallic coordination polymers (HCPs) not only for their fascinating structural topology, but also for their potential applications in magnetism, luminescence materials, molecular adsorption, and bimetallic catalysis [1]. As is well known, according to the hard–soft acid base theory, 3*d* and 4*f* metal ions have different affinities for N and O donors. Generally, 3*d* metal ions easily bond to the ligand containing N donor [2]. However, compared with 3*d* metal ions, 4*f* metal ions more easily bond to the ligand including O donor [1a,1b]. Therefore, if an organic ligand simultaneously contains O and N donors, it should be employed to bond to both 3*d* and 4*f* metal ions to form HCPs. This is a simple and valid method at the present time used to synthesize 3*d*–4*f* HCPs. And, to date, various organic ligands, like pyridinecarboxylate, pyridinephosphonate, imidazolecarboxylate, amino acid, etc., containing O and N donors are selected to construct 3*d*–4*f* HCPs with interesting structures and physico-chemical properties [3]. But the preparation of high dimensional, especially three-dimensional (3D) 3*d*–4*f* HCPs by choosing suitable organic ligands is still a challenge, owing to the following factors: (i) high coordination number and low stereochemical preference for 4*f* metal ions; (ii) the variable and versatile coordination behavior of 3*d* and 4*f* metal ions; and (iii) the competitive reactions between 3*d* and 4*f* metal ions coordinated to the same ligand [4].

On the other hand, pillared-layer approaches to 3D 3*d*–4*f* HCPs has been reported [5]. These existent 3D pillared-layered 3*d*–4*f* frameworks mainly have three following structural models: (i) linkages of coordinated transition-metal (TM) anions acting as pillars and lanthanide (*Ln*)-organic layers [5a,5b]; (ii) linkages of *Ln*-organic pillars and TM-inorganic layers based on inorganic ions (e.g., I^-) having high coordination numbers [5c]; and (iii) organic ligand pillars joining *Ln*-organic layers and TM-inorganic layers [5d]. And it is found that the reported 3D pillared-layer 3*d*–4*f* framework includes at least TM-inorganic layers or *Ln*-organic layers, and the layers are formed by coordination bonding. According to the above pillared-layer structural models, unusual 3D pillared-layer 3*d*–4*f* HCP which is made of one-dimensional (1D) chains or zero-dimensional (0D) clusters of *Ln*-organic and TM-inorganic motifs can be brought to mind. In such structure, *Ln*-organic chains or clusters construct layers via weak bonding interactions (e.g., hydrogen bonding), TM-inorganic sections almost situate in a plane, and organic ligands act as pillars. But, to the best of our knowledge, such pillared-layer structure has never been reported in the literature. If an inorganic ion has no high coordination numbers and organic ligand has proper coordination modes, they can be used to link TM ions and *Ln* ions to produce such pillared-layer structure. This strategy may provide new opportunities for the discovery of interesting structures with particular properties.

Because isonicotinic acid (HIN) is a linear and potentially bridging ligand with O and N donors on opposite sides of the

* Corresponding authors. Fax: +86 5926162225.
E-mail addresses: lqfan@hqu.edu.cn (L.-Q. Fan), jhwu@hqu.edu.cn (J.-H. Wu).

0022-4596/$ - see front matter © 2011 Elsevier Inc. All rights reserved.
doi:10.1016/j.jssc.2011.07.033

molecule as well as the diverse coordination modes, and Br^- ion has smaller ion radius and lower coordination numbers than I^- ion in Cu/X compounds [4c,6], we chose HIN and Br^- ion to synthesize such 3D pillared-layer 3*d*–4*f* HPCs. In this paper, we report the synthesis, crystal structures and properties of two unusual 3D pillared-layer 3*d*–4*f* *Ln*–Cu HCPs, $\{[Ln_2Cu_5Br_4(IN)_7(H_2O)_6]\cdot H_2O\}_n$ (*Ln*=Eu (**1**) and Gd (**2**), HIN=isonicotinic acid), constructed upon the 1D *Ln*–carboxylate chains, 0D $Ln_2(IN)_8$ dimers, rare 1D zigzag $[Cu_5Br_4]_n$ inorganic chains situating in a plane, and IN^- ligands acting as pillars. The 1D *Ln*–carboxylate chains and 0D $Ln_2(IN)_8$ dimers are linked via O–H···O hydrogen bondings to form *Ln*–carboxylate layers.

2. Experimental section

2.1. Materials and methods

All of the reagent-grade reactants were commercially available and employed without further purification. The powder X-ray diffraction (PXRD) data were measured on a DMAX2500 diffractometer. The solid infrared (IR) spectra were obtained from a Nicolet Nexus 470 FT-IR spectrometer between 400 and 4000 cm^{-1} using KBr pellets. Element analyses of carbon, hydrogen and nitrogen were performed with a Vario EL III element analyzer. Thermogravimetric analyses (TGA) were performed on a Netzsch Sta449C thermoanalyzer under air atmosphere in the range of 30–800 °C at a heating rate of 10 °C/min. Fluorescence spectra were obtained at room temperature with the aid of an Edinburgh FLS920 fluorescence spectrophotometer with the polycrystalline sample held between two pieces of fused silica slices. The variable-temperature magnetic susceptibilities were performed with a PPMS-9T magnetometer over the temperature range of 2–300 K under a magnetic field of 1000 Oe. A diamagnetic correction was estimated from Pascal's constants [7]. The crystal structures were determined by a Rigaku Mercury CCD area-detector diffractometer and SHELXL crystallographic software of molecular structure.

2.2. Synthesis of $\{[Ln_2Cu_5Br_4(IN)_7(H_2O)_6]\cdot H_2O\}_n$ (*Ln*=*Eu* (**1**) *and Gd* (**2**))

Compound **1** was hydrothermally synthesized under autogenous pressure. A mixture of Eu_2O_3 (0.176 g, 0.5 mmol), $CuBr_2$ (0.223 g, 1 mmol), HIN (0.246 g, 2 mmol), HNO_3 (0.031 g, 0.5 mmol), and H_2O (10 mL) was stirred at room temperature until a homogeneous mixture was obtained. The mixture was transferred into a Teflon-lined autoclave (23 mL) and heated at 170 °C for 7 days and then cooled at the rate of 2 °C h^{-1} to room temperature. Orange prismatic crystals of **1** were recovered by filtration, washed with distilled water, and dried in air (43% yield based on Eu). Anal. Calcd. for **1** (dried) (%): C, 26.49; H, 2.12; N, 5.15. Found: C, 26.38; H, 2.17; N, 5.21. Selected IR data (KBr pellet, cm^{-1}): 3434, 1605, 1545, 1410, 779.

Compound **2** was prepared with the similar procedure of **1** except that Eu_2O_3 was replaced by Gd_2O_3 (0.181 g, 0.5 mmol). Orange prismatic crystals of **2** were obtained with the yield of 38% based on Gd. Anal. Calcd. for **2** (dried) (%): C, 26.35; H, 2.11; N, 5.12. Found: C, 26.46; H, 2.21; N, 4.96. Selected IR data (KBr pellet, cm^{-1}): 3436, 1597, 1545, 1409, 780.

2.3. Determination of crystal structure

The crystallographic data for **1** and **2** were collected on a Rigaku Mercury CCD area-detector equipped with a graphite-monochromated Mo*K*α radiation (λ=0.71073 Å) at 293(2) K using an $\omega-2\theta$ scan mode. Absorption corrections were performed by the CrystalClear program [8]. Both structures were solved by direct methods using SHELXS-97 program and refined by full-matrix least-squares refinement on F^2 with the aid of SHELXL-97 program [9]. All non-hydrogen atoms were refined anisotropically. Hydrogen atoms attached to carbon were placed in geometrically idealized positions and refined using a riding model. Hydrogen atoms on water molecules were located from the difference in Fourier maps and were also refined using a riding model. Crystallographic data (excluding structure factors) for the

Table 1
Crystallographic data and structure refinement parameters for **1** and **2.**

	1	**2**
Empirical formula	$C_{42}H_{40}Br_4Cu_5Eu_2N_7O_{20}$	$C_{42}H_{40}Br_4Cu_5Gd_2N_7O_{20}$
Formula weight	1904.07	1914.65
Crystal system	Monoclinic	Monoclinic
Space group	*P*2/*c*	*P*2/*c*
a (Å)	17.707(9)	17.702(6)
b (Å)	9.813(4)	9.792(3)
c (Å)	31.918(15)	32.088(11)
β (deg.)	103.362(7)	103.477(7)
V (Å^3)	5396(4)	5409(3)
Z	4	4
T (K)	293(2)	293(2)
$D_{calc.}$ (g cm^{-3})	2.344	2.351
μ (mm^{-1})	7.264	7.380
F(0 0 0)	3648	3656
λ (Å)	0.71073	0.71073
Data collected	33111	33620
Independent data	9465	9400
R_{int}	0.0423	0.0466
θ range (deg.)	2.39–25.00	2.18–25.00
Goodness-of-fit on F^2	1.064	1.076
Data/restraints/parameters	8158/0/724	8060/0/724
R_1 [$I>2\sigma(I)$][a]	0.0450	0.0484
wR_2 [$I>2\sigma(I)$][b]	0.1180	0.1290
$\Delta\rho$ (maximum/minimum) (e Å^{-3})	3.083/−2.512	2.835/−3.120

[a] $R_1=\Sigma||F_0|-|F_c||/\Sigma|F_0|$.
[b] $wR_2=[\Sigma w(|F_0^2|-|F_c^2|)^2/\Sigma w(F_0^2)^2]^{1/2}$.

Table 2
Selected bond lengths (Å) for **1** and **2.**

1			
Eu(1)–O(1)	2.389(5)	Eu(3)–O(18)	2.646(5)
Eu(1)–O(1)#5	2.389(5)	Eu(3)–O(19)	2.449(6)
Eu(1)–O(4)#3	2.375(5)	Cu(1)–Br(1)	2.790(3)
Eu(1)–O(4)#4	2.375(5)	Cu(1)–N(1)	1.948(7)
Eu(1)–O(12)#1	2.336(5)	Cu(1)–N(5)	1.942(7)
Eu(1)–O(12)#2	2.336(5)	Cu(2)–Br(1)	2.505(2)
Eu(1)–O(15)	2.426(5)	Cu(2)–Br(2)	2.4436(19)
Eu(1)–O(15)#5	2.426(5)	Cu(2)–Br(3)	2.872(3)
Eu(2)–O(2)#5	2.320(5)	Cu(2)–N(6)	2.040(6)
Eu(2)–O(2)	2.320(5)	Cu(3)–Br(3)	2.5460(18)
Eu(2)–O(3)#5	2.385(5)	Cu(3)–Br(4)	2.5764(18)
Eu(2)–O(3)	2.385(5)	Cu(3)–Br(5)#10	2.4873(19)
Eu(2)–O(11)#6	2.403(5)	Cu(3)–N(2)	2.035(7)
Eu(2)–O(11)#7	2.403(5)	Cu(4)–Br(4)	2.6417(16)
Eu(2)–O(16)	2.567(5)	Cu(4)–N(3)	1.962(6)
Eu(2)–O(16)#5	2.567(5)	Cu(4)–N(7)	1.961(6)
Eu(3)–O(6)	2.319(5)	Cu(5)–Br(1)#10	2.3729(19)
Eu(3)–O(7)#8	2.319(5)	Cu(5)–Br(3)#10	2.710(2)
Eu(3)–O(8)	2.367(5)	Cu(5)–Br(5)	2.5665(18)
Eu(3)–O(10)#9	2.378(5)	Cu(5)–N(4)	2.005(7)
Eu(3)–O(13)#7	2.472(5)	Cu(3)–Cu(5)#10	2.666(2)
Eu(3)–O(17)	2.426(6)		
2			
Gd(1)–O(1)	2.380(5)	Gd(3)–O(18)	2.633(5)
Gd(1)–O(1)#5	2.380(5)	Gd(3)–O(19)	2.432(6)
Gd(1)–O(4)#3	2.357(5)	Cu(1)–Br(1)	2.792(2)
Gd(1)–O(4)#4	2.357(5)	Cu(1)–N(1)	1.946(7)
Gd(1)–O(12)#1	2.321(5)	Cu(1)–N(5)	1.934(7)
Gd(1)–O(12)#2	2.321(5)	Cu(2)–Br(1)	2.4964(18)
Gd(1)–O(15)	2.431(5)	Cu(2)–Br(2)	2.4480(18)
Gd(1)–O(15)#5	2.431(5)	Cu(2)–Br(3)	2.902(3)
Gd(2)–O(2)	2.311(5)	Cu(2)–N(6)	2.037(6)
Gd(2)–O(2)#5	2.311(5)	Cu(3)–Br(3)	2.5617(18)
Gd(2)–O(3)	2.379(5)	Cu(3)–Br(4)	2.5890(17)
Gd(2)–O(3)#5	2.379(5)	Cu(3)–Br(5)#10	2.4939(18)
Gd(2)–O(11)#6	2.398(5)	Cu(3)–N(2)	2.022(7)
Gd(2)–O(11)#7	2.398(5)	Cu(4)–Br(4)	2.6361(14)
Gd(2)–O(16)#5	2.547(5)	Cu(4)–N(3)	1.951(6)
Gd(2)–O(16)	2.547(5)	Cu(4)–N(7)	1.960(6)
Gd(3)–O(6)	2.313(5)	Cu(5)–Br(1)#10	2.3822(19)
Gd(3)–O(7)#8	2.304(5)	Cu(5)–Br(3)#10	2.710(2)
Gd(3)–O(8)	2.355(5)	Cu(5)–Br(5)	2.5803(18)
Gd(3)–O(10)#9	2.371(6)	Cu(5)–N(4)	2.002(7)
Gd(3)–O(13)#7	2.467(5)	Cu(3)–Cu(5)#10	2.675(2)
Gd(3)–O(17)	2.439(6)		

Symmetry codes for **1**: #1 $1-x$, $-1+y$, $1/2-z$; #2 $-1+x$, $-1+y$, z; #3 $-x$, $-1+y$, $1/2-z$; #4 x, $-1+y$, z; #5 $-x$, y, $1/2-z$; #6 $1-x$, y, $1/2-z$; #7 $-1+x$, y, z; #8 $-x$, $2-y$, $1-z$; #9 $-1+x$, $1+y$, z; #10 $1-x$, $2-y$, $1-z$. Symmetry codes for **2**: #1 $1-x$, $1+y$, $1/2-z$; #2 $-1+x$, $1+y$, z; #3 x, $1+y$, z; #4 $-x$, $1+y$, $1/2-z$; #5 $-x$, y, $1/2-z$; #6 $1-x$, y, $1/2-z$; #7 $-1+x$, y, z; #8 $-x$, $1-y$, $1-z$; #9 $-1+x$, $-1+y$, z; #10 $1-x$, $1-y$, $1-z$.

structure reported in this paper have been deposited with the Cambridge Crystallographic Data Centre as supplementary publication nos. CCDC 822688 for **1** and 822689 for **2**. Copies of the data can be obtained free of charge on application to CCDC, 12 Union Road, Cambridge CB2 1EZ, UK (fax: +44 1223 336 033; e-mail: deposit@ccdc.cam.ac.uk). Some refinement details and crystal data of **1** and **2** are summarized in Table 1. Selected bond lengths of **1** and **2** are shown in Table 2. Selected bond angles of **1** and **2** are gathered in Table S1 in the Supplementary Materials.

3. Results and discussion

3.1. Synthesis

The compounds **1** and **2** were synthesized from the reaction mixture of Ln_2O_3, $CuBr_2$, HIN, and HNO_3 with the mole ratio of 1:2:4:1 in water at 170 °C by the hydrothermal technique. In this system, HNO_3 was added to adjust the pH value of the reaction mixture. And it was found that crystals suitable for X-ray single-crystal analysis were obtained only with this ratio. However, isomorphous compounds with other Ln^{3+} having larger or smaller ion radii are not obtained. Series of experiments using Cl^- and I^- ions as halide sources in place of Br^- ion have been carried out to prepare compounds similar in structure to these two compounds, but unfortunately, we were unsuccessful. The main reason may be that Cl^- and I^- have smaller and larger ion radii than Br^-, respectively, which do not favor proper coordination numbers that benefit to give rise to such a 3D pillared-layer network.

3.2. Structure description

Single-crystal X-ray diffraction analyses reveal that **1** and **2** crystallize in the monoclinic space group $P2/c$ and possess unusual 3D pillared-layer framework. Because **1** and **2** are isostructural, only the structure of **1** is described in detail. An ORTEP view of **1** is shown in Fig. 1. The asymmetric unit of **1** contains one Eu^{3+} ion in general position and two half Eu^{3+} ions: one lies about an inversion center while the other lies about a twofold axis, three Br^- ions in general position and two half Br^- ions: one locates about an inversion center while the other locates about a twofold axis, five Cu^+ ions, seven IN^- ligands, five coordinated water molecules and one uncoordinated water molecule, all in general position. The Eu(1), Eu(2) and Eu(3) centers all are eight-coordinated and display bicapped trigonal prismatic coordination environment: six oxygen atoms from six IN^- ligands, two oxygen atoms from two coordinated water molecules for the Eu(1) and Eu(2) centers; five oxygen atoms from five IN^- ligands, three oxygen atoms from three coordinated water molecules for the Eu(3) center. The Eu–O bond lengths vary from 2.319(5) to 2.646(5) Å, and the O–Eu–O bond angles are in the range of 66.81(18)–148.36(18)°, thus being in the normal range observed in

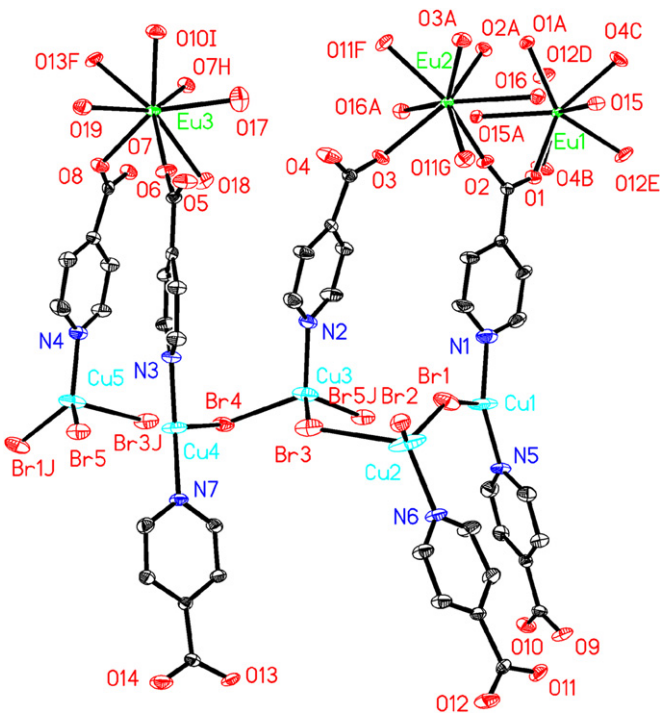

Fig. 1. ORTEP plot of the asymmetric unit of **1** (30% probability ellipsoids). All H atoms and uncoordinated water molecule are omitted for clarity. Symmetry codes: A: $-x$, y, $1/2-z$; B: x, $-1+y$, z; C: $-x$, $-1+y$, $1/2-z$; D: $-1+x$, $-1+y$, z; E: $1-x$, $-1+y$, $1/2-z$; F: $-1+x$, y, z; G: $1-x$, y, $1/2-z$; H: $-x$, $2-y$, $1-z$; I: $-1+x$, $1+y$, z; J: $1-x$, $2-y$, $1-z$.

other compounds [2b,10]. Both Cu(1) and Cu(4) centers exhibit trigonal conformation, being coordinated by two nitrogen atoms from two different IN^- ligands and one Br^- ion. However, all Cu(2), Cu(3) and Cu(5) centers present tetrahedral geometry, being bonded by one nitrogen atom from IN^- ligand and three Br^- ions. The Cu–N and Cu–Br bond lengths range from 1.942(7) to 2.040(6) Å and from 2.3729(19) to 2.872(3) Å, respectively, all within the range of those observed for other *Ln*–Cu compounds [4c,6c,6d]. In this structure, the IN^- ligands have two evidently different coordination modes: one behaves as a bridging ligand to coordinate two Eu^{3+} ions and one Cu^+ ion (Scheme 1a), another also behaves as a bridging ligand, but it coordinates one Eu^{3+} ion and one Cu^+ ion (Scheme 1b). Although Cu^{2+} ions were used as starting materials in **1** and **2**, the Cu centers have an oxidation state of +1, attributed to a reduction reaction involving the IN^- ligands [4c,6c,11], and is consistent with the geometry of the Cu^+ ions and evidenced by the orange color of crystals, which is further corroborated by the bond valence sum calculations with the valences of Cu(1), Cu(2), Cu(3), Cu(4) and Cu(5) being 0.98, 1.04, 1.09, 1.01 and 1.12, respectively [12].

The Eu(1) and Eu(2) centers are alternately bridged by two and four μ-carboxylate groups of IN^- ligands in a 4–2–4–2 (the number indicates the number of the bridges) mode to construct a 1D linear Eu–carboxylate chain along *b*-axis with the Eu···Eu distances of 4.549(2) and 5.264(2) Å, respectively (Fig. 2a), and the Eu···Eu···Eu angles of 180°. Eu(3) and its symmetry related center are linked by two μ-carboxylate groups of IN^- ligands to form a 0D *Ln*–carboxylate $Eu_2(IN)_8$ dimer with a Eu···Eu distance of 5.149(2) Å (Fig. 2b).

$Cu(2)Br_3N$, $Cu(3)Br_3N$ and $Cu(5)Br_3N$ tetrahedra connect each other by common edges (Br(1)–Br(3), Br(3)–Br(5)) to form trimer with the Cu(3)–Cu(5) distance of 2.666(2) Å, which is much shorter than the double van der Waals radius of the Cu^+ ion (1.4 Å) [6c], implying a strong Cu–Cu interaction. The trimer links two triangles ($Cu(1)BrN_2$, $Cu(4)BrN_2$) through common vertices (Br(1), Br(4)) to generate a pentanuclear Cu cluster. And then the pentanuclear Cu cluster is connected with its symmetry-related structure by sharing vertex (Br(4)) to produce octanuclear Cu cluster. Neighboring octanuclear Cu clusters further link each other by common vertex (Br(2)) to give rise to rare 1D zigzag $[Cu_5Br_4]_n$ inorganic chains extending along *c*-axis (Fig. 3). The 1D zigzag $[Cu_5Br_4]_n$ inorganic chains parallel to each other extending along *bc* plane. As a consequence of the connectivity of $CuBr_3N$ tetrahedra and $CuBrN_2$ triangles in **1**, the Br^- ions act as μ_2 (Br(2), Br(5)), μ_3 (Br(1), Br(3)) and μ_4 (Br(4)) ligands. The linkages of 1D linear Eu–carboxylate chains, 0D $Eu_2(IN)_8$ dimers and $[Cu_5Br_4]_n$ inorganic chains by IN^- pillars construct such a novel 3D framework (Fig. 4). In this 3D structure, it is noticed that the 1D Eu–carboxylate chains and $Eu_2(IN)_8$ dimers are joined by weak O–H···O hydrogen bondings to produce 2D Eu–carboxylate layers extending along *bc* plane (Fig. 5), which is different from that in other pillared-layer 3*d*–4*f* HCPs. And the 2D Eu–carboxylate layer is further stabilized by the uncoordinated water molecules situating between 1D Eu–carboxylate chains and $Eu_2(IN)_8$ dimers through O–H···O hydrogen bondings (Table S2 for **1** and S3 for **2** in Supplementary Materials).

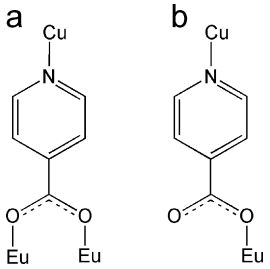

Scheme 1. Coordination modes of the IN^- ligand in **1**.

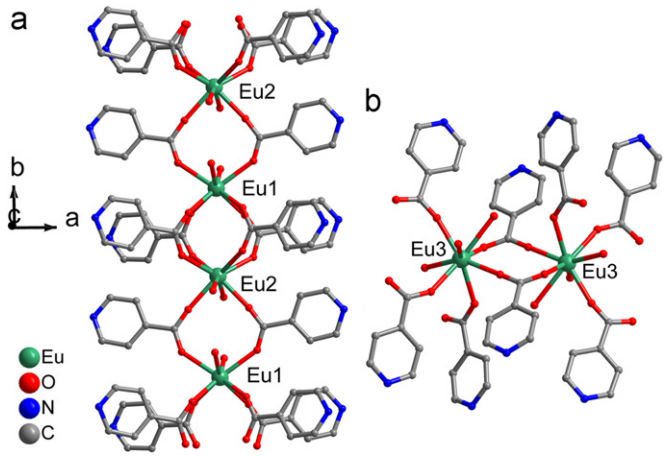

Fig. 2. (a) View of the 1D Eu–carboxylate chain of **1** along *b*-axis. (b) View of $Eu_2(IN)_8$ dimer.

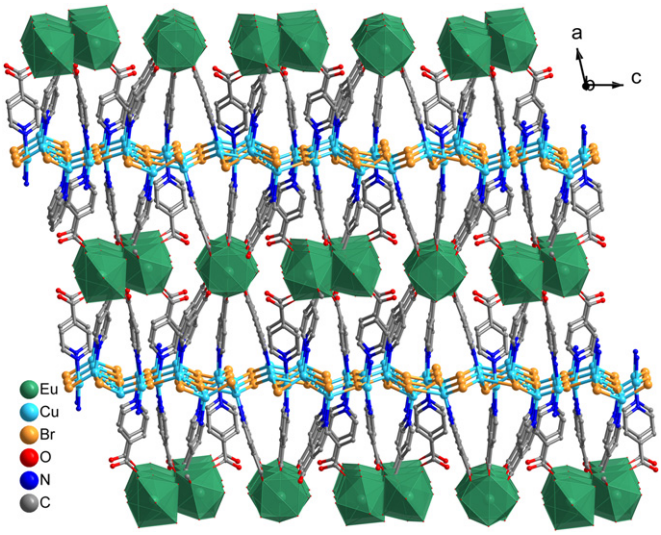

Fig. 4. Packing diagram of **1** viewed approximately down the [010] direction. All H atoms and uncoordinated water molecules are omitted for clarity.

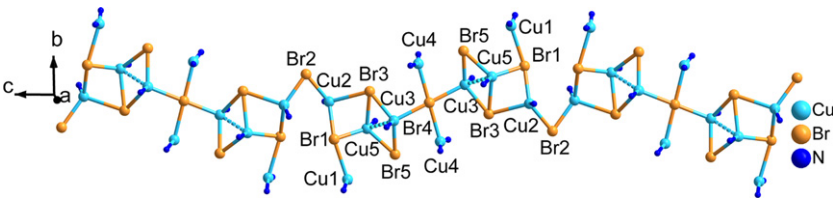

Fig. 3. Diagram of $[Cu_5Br_4]_n$ inorganic chain of **1** along *c*-axis.

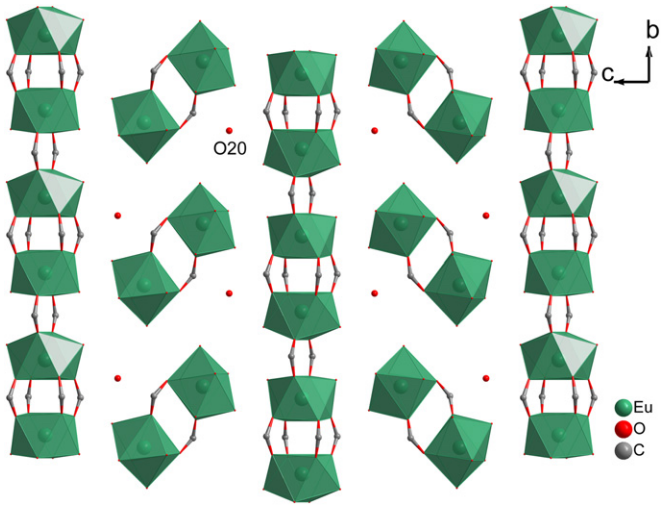

Fig. 5. Polyhedral diagram of 2D Eu–carboxylate layer extending along *bc* plane.

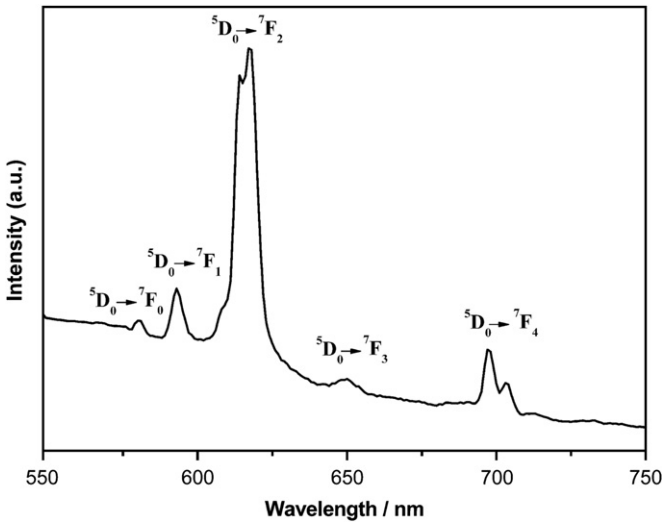

Fig. 6. Solid-state emission spectrum for **1** in the solid state at room temperature (excited at 292 nm).

3.3. PXRD analysis

The as-synthesized samples of **1** and **2** were characterized by powder X-ray diffraction at room temperature. The PXRD patterns for the bulk product are in fair agreement with the patterns based on single-crystal X-ray solution in position, indicating the phase purity of the as-synthesized samples of **1** and **2** (see Figs. S1 and S2 in the Supplementary Materials). The difference in reflection intensities between the simulated and experimental patterns was due to the variation in preferred orientation of the powder sample during collection of the experimental PXRD data.

3.4. IR spectroscopy

In the IR spectrum of **1** (see Fig. S3(a) in the Supplementary Materials), the strong and broad absorption band in the range of about 3434 cm^{-1} is assigned as a characteristic peak of OH vibration. The strong vibrations appearing at 1605 and 1410 cm^{-1} correspond to the asymmetric and symmetric stretching vibrations of carboxylate group, respectively. The absence of strong bands in the range of 1690–1730 cm^{-1} indicates that all carboxyl groups of HIN are deprotonated [13]. The IR spectrum of **2** exhibits similar feature as that of **1** (see Fig. S3(a) and (b) in the Supplementary Materials).

3.5. Thermal stability

The thermal stability of **1** and **2** was examined by TGA in air atmosphere from 30 to 800 °C (see Figs. S4 and S5 the Supplementary Materials). They show the similar thermal behavior. The lattice-water and coordinated water molecules were gradually lost in the temperature range of 30–241 °C (calcd./found: 5.67/5.53% for **1**, 5.64/5.35% for **2**). Above this temperature, the weight loss is due to the decomposition of the IN^- ligands and the collapse of the whole framework of these two compounds; and the final residue after heating to 800 °C had a composition of $Ln_2O_3 \cdot 5(CuO)$ (calcd./found: 39.31/38.53% for **1**, 39.70/39.26% for **2**).

3.6. Luminescent properties

Because of the excellent luminescent properties of Eu^{3+} ions, the luminescent properties of **1** in solid state were investigated at room temperature. As shown in Fig. 6, the emission spectrum of **1** with an excitation wavelength of 292 nm displays the characteristic transitions of $^5D_0 \rightarrow {}^7F_n$ ($n=0 \rightarrow 4$) of Eu^{3+} ions at 580, 593, 617, 649, and 698 nm, respectively [14]. The appearance of the symmetry-forbidden emission $^5D_0 \rightarrow {}^7F_0$ at 580 nm indicates that Eu^{3+} ions occupy sites with low symmetry and without an inversion center, which is confirmed by X-ray structural structure of **1**. The band at 593 nm can be attributed to magnetic-dipolar $^5D_0 \rightarrow {}^7F_1$ transition. And the band at 617 nm can be assigned to electric-dipolar $^5D_0 \rightarrow {}^7F_2$ transition. The intensity of the $^5D_0 \rightarrow {}^7F_2$ transition increases with the decrease of the site symmetry of Eu^{3+} ions. The intensity ratio of $I(^5D_0 \rightarrow {}^7F_2)/I(^5D_0 \rightarrow {}^7F_1)$ is equal to ca. 2.57, which also denotes the noncentrosymmetric coordination geometry of the Eu^{3+} ions in **1**. The most intense transition is $^5D_0 \rightarrow {}^7F_2$, which implies intense red luminescence of **1**. It can be found that, in **1**, ligand-to-copper energy transfer is unobvious, which is testified by no other emission peaks existing in the emission spectrum except the characteristic emission peaks of Eu^{3+} ions.

3.7. Magnetic properties

The magnetic susceptibilities of **1** and **2** have been measured from ground crystals under a constant magnetic field of 1000 Oe over the temperature range of 2–300 K. The data are presented as plots of χ_M^{-1} vs. T and $\chi_M T$ vs. T (χ_M being molar magnetic susceptibility per Ln^{3+} ion) in Figs. 7 and 8 for **1** and **2**, respectively. For **1**, the observed $\chi_M T$ at room temperature is 1.43 $cm^3\ K\ mol^{-1}$, slightly less than the value 1.5 for a free Eu^{3+} ion calculated by Van Vleck allowing for population of the excited state with higher values of J at 300 K. As the temperature is lowered, $\chi_M T$ decreases continuously, which should be attributed to the depopulation of the Stark levels for a single Eu^{3+} ion. At the lowest temperature of 2 K, $\chi_M T$ is close to zero, indicating a $J=0$ ground state of the Eu^{3+} ion ($^7F_0$). The magnetic susceptibility above 150 K follows the Curie–Weiss law due to the presence of thermally populated excited states [15].

For **2**, the value of $\chi_M T$ at 300 K is 7.72 $cm^3\ K\ mol^{-1}$ which is close to the value for one free Gd^{3+} ion ($\chi_M T=7.88\ cm^3\ K\ mol^{-1}$, $g=2$). Upon cooling, the value of $\chi_M T$ slowly increases up to a maximum of 8.61 $cm^3\ K\ mol^{-1}$ at ca. 15 K, and then abruptly decreases down to a minimum 7.87 $cm^3\ K\ mol^{-1}$ at 2 K. The thermal evolution of χ_M^{-1} obeys the Curie–Weiss law, $\chi_M = C/(T-\theta)$, over the temperature range from 50 to 300 K with $C=7.58\ cm^3\ K\ mol^{-1}$, $\theta=8.65$ K. All these results suggest that a ferromagnetic coupling between Gd^{3+} ions exists in **2** although the Gd···Gd distance is between 4.54 and 5.26 Å [16]. The carboxyl bridge may provide an effective interaction path for the ferromagnetic coupling.

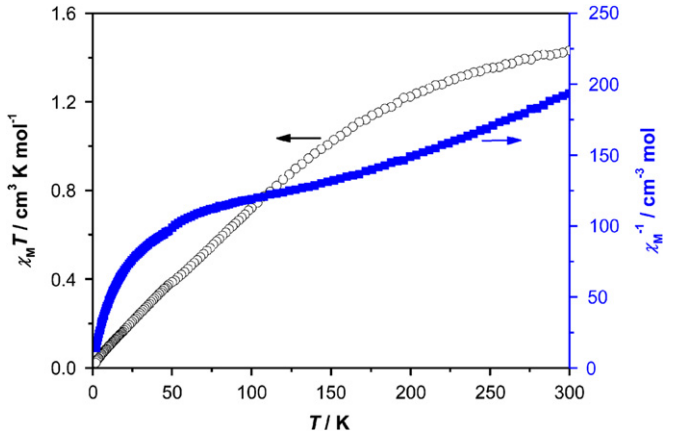

Fig. 7. Plots of χ_M (■) and $\chi_M T$ (○) vs. T of **1** over the temperature of 2–300 K at the field of 1000 Oe.

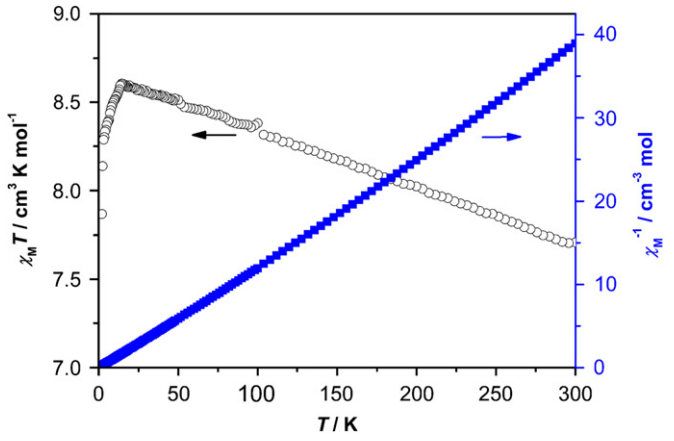

Fig. 8. Plots of χ_M (■) and $\chi_M T$ (○) vs. T of **2** over the temperature of 2–300 K at the field of 1000 Oe.

4. Conclusions

In conclusion, two unusual 3D pillared-layer 3*d*–4*f* *Ln*–Cu HCPs built upon the linkages of 1D linear *Ln*–carboxylate chains, 0D $Ln_2(IN)_8$ dimer, 1D zigzag $[Cu_5Br_4]_n$ inorganic chains and IN^- pillars have been obtained and characterized by X-ray diffraction, thermal analysis, IR, luminescence and magnetic properties. The key point of the synthetic procedures has been well-established. The work opens new perspective and a feasible synthetic strategy for the construction of such 3D pillared-layer 3*d*–4*f* HCPs with particular functions; work is continuing in this area.

Acknowledgments

This work was supported financially by the National High Technology Research and Development Program of China (863 Program) (No. 2009AA03Z217), the National Natural Science Foundation of China (No. 90922028), the Key Project of Chinese Ministry of Education (No. 211204) and the Fund of Fujian Provincial Key Laboratory of Nanomaterials (No. NM10-5).

Appendix A. Supplementary data

Selected bond angles, hydrogen bonding distances and angles, simulated and experimental PXRD patterns, IR spectra, and TG curves for **1** and **2** are provided as supplementary materials.

Appendix A. Supporting information

Supplementary data associated with this article can be found in the online version at doi:10.1016/j.jssc.2011.07.033.

References

[1] (a) M. Shibasaki, N. Yoshikawa, Chem. Rev. 102 (2002) 2187;
(b) J. Inanaga, H. Furuno, T. Hayano, Chem. Rev. 102 (2002) 2211;
(c) J.P. West, W.L. Queen, S.J. Hwu, K.E. Michaux, Angew. Chem. Int. Ed. 50 (2011) 3780;
(d) V. Mereacre, Y. Lan, R. Clérac, A.M. Ako, I.J. Hewitt, W. Wernsdorfer, G. Buth, C.E. Anson, A.K. Powell, Inorg. Chem. 49 (2010) 5293;
(e) X.Q. Zhao, Y.H. Lan, B. Zhao, P. Cheng, C.E. Anson, A.K. Powell, Dalton Trans. 39 (2010) 4911;
(f) Y.M. Xie, W.T. Chen, J.H. Wu, J. Solid State Chem. 181 (2008) 1853;
(g) F.C. Liu, Y.F. Zeng, J. Jiao, J.R. Li, X.H. Bu, J. Ribas, S.R. Batten, Inorg. Chem. 45 (2006) 6129;
(h) K.C. Mondal, O. Sengupta, P. Dutta, M. Seehra, S.K. Nayak, P.S. Mukherjee, Inorg. Chim. Acta 362 (2009) 1913;
(i) Y.P. Yuan, R.Y. Wang, D.Y. Kong, J.G. Mao, A. Clearfield, J. Solid State Chem. 178 (2005) 2030;
(j) M. Andrun, Chem. Commun. (2011) 3025.
[2] (a) J.P. Zhang, X.M. Chen, J. Am. Chem. Soc. 131 (2009) 5516;
(b) J.W. Cheng, S.T. Zheng, G.Y. Yang, Dalton Trans. (2007) 4059;
(c) L.Q. Fan, J.H. Wu, Y.F. Huang, J. Solid State Chem. 180 (2007) 3479;
(d) L.Q. Fan, J.H. Wu, Y.F. Huang, J.M. Lin, Solid State Sci. 12 (2010) 558;
(e) X. Hu, Y.F. Zeng, Z. Chen, E.C. Sanudo, F.C. Liu, J. Ribas, X.H. Bu, Cryst. Growth Des. 9 (2009) 421.
[3] (a) F. Luo, D.X. Hu, L. Xue, Y.X. Che, J.M. Zheng, Cryst. Growth Des. 7 (2007) 851;
(b) X.J. Gu, D.F. Xue, Growth Des. 7 (2007) 1726;
(c) Z.Y. Li, N. Wang, J.W. Dai, S.T. Yue, Y.L. Liu, CrystEngComm 11 (2009) 2003;
(d) Y.S. Ma, Y. Song, L.M. Zheng, Inorg. Chim. Acta 361 (2008) 1363;
(e) Q. Zhang, Y.X. Zheng, C.X. Liu, Y.G. Sun, E.J. Gao, Inorg. Chem. Commun. 12 (2009) 523;
(f) N.F. Chilton, S.K. Langley, B. Moubaraki, K.S. Murray, Chem. Commun. (2010) 7787;
(g) J.J. Zhang, S.M. Hu, S.C. Xiang, T.L. Sheng, X.T. Wu, Y.M. Li, Inorg. Chem. 45 (2006) 7173.
[4] (a) Y.P. Ren, L.S. Long, B.W. Mao, Y.Z. Yuan, R.B. Huang, L.S. Zheng, Angew. Chem. Int. Ed. 42 (2003) 532;
(b) F. Luo, Y.X. Che, J.M. Zheng, Cryst. Growth Des. 6 (2006) 2432;
(c) J.W. Cheng, S.T. Zheng, G.Y. Yang, Inorg. Chem. 46 (2007) 10261;
(d) X.J. Gu, D.F. Xue, Inorg. Chem. 46 (2007) 5349;
(e) J.W. Cheng, S.T. Zheng, G.Y. Yang, Inorg. Chem. 47 (2008) 4930;
(f) M.Y. Li, Y.H. Lan, A.M. Ako, W. Wernsdorfer, C.E. Anson, G. Buth, A.K. Powell, Z.M. Wang, S. Gao, Inorg. Chem. 49 (2010) 11587.
[5] (a) J.W. Cheng, S.T. Zheng, E. Ma, G.Y. Yang, Inorg. Chem. 46 (2007) 10534;
(b) Y.W. Li, Y.H. Wang, Y.G. Li, E.B. Wang, J. Solid State Chem. 181 (2008) 1485;
(c) L.Q. Fan, Y. Chen, J.H. Wu, Y.F. Huang, J. Inorg. Organomet. Polym. 21 (2011) 346;
(d) J.W. Cheng, J. Zhang, S.T. Zheng, G.Y. Yang, Chem. Eur. J. 14 (2008) 88.
[6] (a) L.Q. Fan, L.M. Wu, L. Chen, Inorg. Chem. 45 (2006) 3149;
(b) Q. Hou, J.N. Xu, J.H. Yu, T.G. Wang, Q.F. Yang, J.Q. Xu, J Solid State Chem. 183 (2010) 1561;
(c) H. Deng, Z.H. Liu, Y.C. Qiu, Y.H. Li, M. Zeller, Inorg. Chem. Commun. 11 (2008) 978;
(d) Z.B. Zhu, H.P. Zeng, J. Coord. Chem. 63 (2010) 2097.
[7] O. Kahn, Molecular Magnetism, VCH, Weinheim, Germany, 1993.
[8] Rigaku, CrystalClear, version 1.3.6, Rigaku/MSC, Tokyo, Japan, 2005.
[9] (a) G.M. Sheldrick, SHELXS-97, Program for the Solution of Crystal Structures, University of Göttingen, Germany, 1997;
(b) G.M. Sheldrick, SHELXL-97, Program for the Refinement of Crystal Structures, University of Göttingen, Germany, 1997.
[10] L.Q. Fan, Y. Chen, J.H. Wu, Y.F. Huang, J. Solid State Chem. 184 (2011) 899.
[11] W.Y. Xiao, X.J. Gu, D.F. Xue, J. Cryst. Growth 311 (2009) 601.
[12] I.D. Brown, D. Altermatt, Acta Crystallogr. Sect. B 41 (1985) 244.
[13] (a) X.J. Gu, D.F. Xue, CrystEngComm 9 (2007) 471;
(b) Y.C. Qiu, Z.H. Liu, J.X. Mou, H. Deng, M. Zeller, CrystEngComm 12 (2010) 277.
[14] (a) A. Bettencourt-Dias, S. Vsiwanathan, Chem. Commun. (2004) 1024;
(b) M.S. Chen, Z. Su, M. Chen, S.S. Chen, Y.Z. Li, W.Y. Sun, CrystEngComm 12 (2010) 3267.
[15] (a) Y.H. Wan, L.P. Zhang, L.P. Jin, S. Gao, S.Z. Lu, Inorg. Chem. 42 (2003) 4985;
(b) Z. He, E.Q. Gao, Z.M. Wang, C.H. Yan, M. Kurmoo, Inorg. Chem. 44 (2005) 862.
[16] (a) P.F. Yan, F.M. Zhang, G.M. Li, J.W. Zhang, W.B. Sun, M. Suda, Y. Einaga, J. Solid State Chem. 182 (2009) 1685;
(b) Z.Y. Li, J.W. Dai, N. Wang, H.H. Qiu, S.T. Yue, Y.L. Liu, Cryst. Growth Des. 10 (2010) 2746.